Chronic imaging of cortical oxygen tension and blood flow after targeted vascular occlusion

Colin T. Sullender[a], Andrew E. Mark[a], Taylor A. Clark[b,c], Tatiana V. Esipova[d], Sergei A. Vinogradov[d], Theresa A. Jones[b,c], Andrew K. Dunn[a,c*]

[a]The University of Texas at Austin, Department of Biomedical Engineering, 107 W. Dean Keeton St. Stop C0800, Austin, TX, 78712, USA

[b]The University of Texas at Austin, Department of Psychology, 108 W. Dean Keeton St. Stop A8000, Austin, TX, 78712, USA

[c]The University of Texas at Austin, Institute for Neuroscience, 1 University Station Stop C7000, Austin, Texas 78712, USA

[d]University of Pennsylvania, Department of Biochemistry and Biophysics, Philadelphia, PA, 19104, USA

Abstract. We present a dual-modality imaging system combining laser speckle contrast imaging and phosphorescence lifetime quenching to simultaneously map cortical blood flow and oxygen tension (pO_2) in mice. Phosphorescence signal localization is achieved through the use of a digital micromirror device (DMD) that allows for selective excitation of arbitrary regions of interest. By targeting both excitation maxima of the oxygen-sensitive porphyrin Oxyphor PtG4, we are able to examine the effects of excitation wavelength and penetration depth on phosphorescence lifetime. We demonstrate the ability to measure differences in pO_2 between arteries and veins and large changes during an hyperoxic challenge. We dynamically monitor blood flow and pO_2 during DMD-targeted photothrombotic occlusion of an arteriole and highlight the presence of an ischemia-induced depolarization. Chronic tracking of the ischemic lesion over eight days revealed a rapid recovery, with the targeted vessel fully reperfusing and pO_2 returning to baseline values within five days. This system has broad applications for studying the acute and chronic pathophysiology of ischemic stroke and other vascular diseases of the brain.

Keywords: laser speckle contrast imaging, oxygen tension, phosphorescence quenching, photothrombosis, ischemic stroke, imaging system.

*Andrew K. Dunn adunn@utexas.edu

1 Introduction

The measurement of blood flow and oxygen tension in cerebral vasculature is vital for the study of many physiological and pathophysiological conditions in the brain. Laser speckle contrast imaging (LSCI) is a well-established technique for full-field optical imaging of cortical blood flow.[1–4] *In vivo* measurements of molecular oxygen have historically been made using highly invasive Clarke electrodes that are limited to point measurements outside the vascular lumen.[5–7] Magnetic resonance techniques allow for noninvasive imaging of hemoglobin saturation, but suffer from low spatial resolutions and can only be correlated with free oxygen in the blood.[7–11] Oxygen-sensitive

porphyrin probes allow for noninvasive, highly sensitive optical oxygenation measurements based on phosphorescence quenching.[12] While an injection of the probe is required, absolute oxygen tension (pO_2) can be directly calculated from the lifetime of the measured phosphorescence decay.

In order to spatially resolve the phosphorescent signal, most lifetime imaging systems utilize intensified exposure-gated cameras[13,14] or laser scanning systems,[15,16] both of which have limitations.[17] Cameras suffer from poor spatial resolution because of light scattering in tissue while scanning systems lack temporal resolution because each spatial location requires many repeated measurements. The use of a digital micromirror device (DMD) as a spatial light modulator was proposed to overcome these limitations.[18] Rather than producing a full image, arbitrary regions of interest could be sequentially targeted for selective excitation. By constraining the phosphorescent signal to only the targeted region, a point detector could be used for acquiring spatially-resolved lifetime data with high sensitivity and temporal resolution.

In this paper we present an update to the system by Ponticorvo and Dunn[18] that utilizes a more robust porphyrin probe[19] and offers higher spatiotemporal resolutions for both LSCI and phosphorescence lifetime imaging. Using both of the phosphorescent probe's excitation maxima, we highlight wavelength-dependent differences in measured decay lifetimes. We demonstrate the ability to detect static variations in pO_2 between different types of vasculature and the dynamic monitoring of blood flow and pO_2 during DMD-targeted photothrombotic stroke. We also demonstrate chronic imaging by tracking the response to an ischemic event over several days. This system allows for acute and chronic imaging of relative blood flow and oxygen tension and has broad applications for both basic neuroscience and neuropathophysiology.

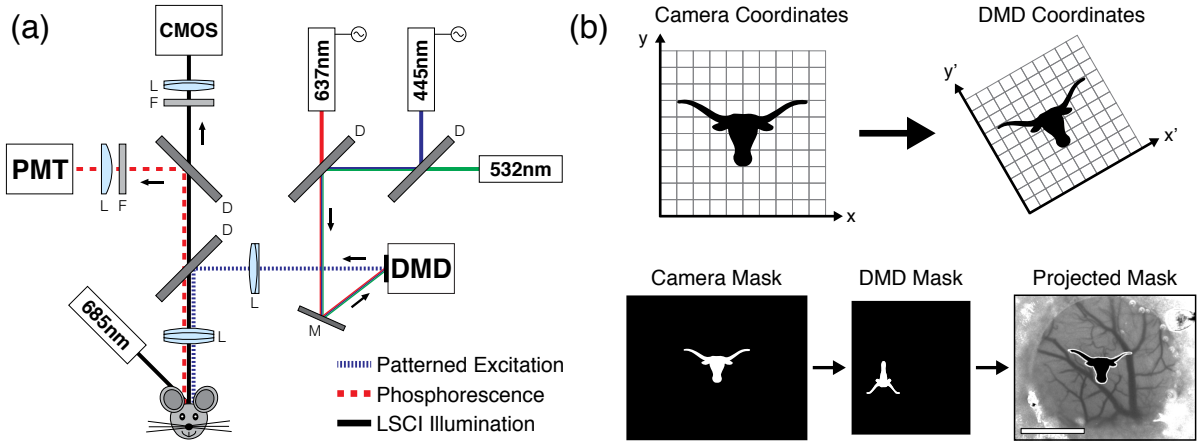

Fig 1 (a) Schematic of the imaging system. Three diode lasers (445, 532, and 637 nm) are coaligned and coupled with the DMD to provide structured illumination onto a cranial window. A separate 685 nm laser provides oblique illumination for LSCI. A pair of dichroic beamsplitters separate phosphorescence from scattered LSCI laser light for detection. (b) Example of the linear image transformation applied to binary masks for DMD patterning and the resulting projection as imaged using LSCI (Scale bar = 1 mm).

2 Methods

2.1 Imaging Instrumentation

A schematic of the imaging system is presented in Fig. 1a. LSCI was performed using a 685 nm laser diode (50 mW, HL6750MG, Thorlabs) illuminating the craniotomy at an oblique angle. The excitation and emission spectra of the phosphorescent probe dictated dichroic beamsplitter cutoff wavelengths and limited the options for the near-infrared laser diode wavelength. The scattered light was relayed to a CMOS camera (acA1300-60gmNIR, 1280 x 1024 pixels, Basler AG) with 2x magnification for a field of view of 3.5 mm x 2.8 mm. Images were acquired using custom software written in C++ at 60 frames per second with a 5 ms exposure time.

Simultaneously, laser light patterned by the DMD was delivered to the craniotomy to selectively excite the phosphorescent probe. Wavelength has been shown to significantly affect the penetration depth and sampled volume of measurements through surface vasculature,[20] so two different lasers at 445 nm (200 mW, AixiZ) and 637 nm (250 mW, HL6388MG, Thorlabs) were selected

to target the Soret and Q band excitation maxima of the dye.[19] Each laser was used independently to collect lifetime measurements from identical regions of interest for comparison. The 445 nm laser was gated using an acousto-optic modulator (23080-2-LTD, Neos Technologies) while the 637 nm laser was directly gated via its driver (LDD400-1P, Wavelength Electronics). Both lasers were gated to produce 20 μs pulses of light for time domain lifetime measurements with a 6% duty cycle and approximately 3 kHz repetition rate using an National Instruments FlexRIO FPGA (NI PXIe-7965R and NI 5781) for waveform generation.

The modulated laser light was relayed to a DMD for projection onto the craniotomy. A DMD is an optical semiconductor device that consists of a two-dimensional array of thousands of individually addressable mirrors that can be tilted to spatially modulate light. The DMD allows for the localization of phosphorescence measurements while maintaining the high sensitivity of using a point detector.[18] A DLP LightCrafter Evaluation Module (Texas Instruments) was modified to expose the bare DMD (DLP3000, 608 x 684 pixels, 7.6 μm pitch) for illumination. The projected DMD pattern was co-registered with the LSCI camera via an affine image transformation (Fig. 1b). This allowed for the selection of arbitrarily-shaped regions of interest using speckle contrast imagery for guidance. The resulting binary masks were then transformed into DMD coordinate space and uploaded onto the device via its USB-based API. Each pattern was then projected sequentially onto the exposed brain tissue to selectively excite the phosphorescent probe for pO_2 measurements.

The emitted phosphorescence was separated from the excitation light and LSCI laser using a pair of dichroic beamsplitters (650 nm, ZT640rdc, Chroma Technology and 750 nm, FF750-SDi02, Semrock) and a bandpass filter (775$\pm$26 nm, 84-106, Edmund Optics) and relayed to a photomultiplier tube for detection (H7422P-50, Hamamatsu Photonics). The analog signal was digitized at 100 MHz and accumulated by the FPGA for averaging, after which it was transferred to

the host computer and written to file. The maximum pattern projection rate and temporal resolution of the pO_2 measurements were limited by the averaging of the phosphorescent decays. In order to balance the signal-to-noise ratio and speed, patterns were displayed at 10 Hz with 200 decays collected during each projection. While faster pattern rates were possible (e.g. 50 Hz with 40 decays averaged), the reduction in averaging negatively affected the quality of the recorded decays.

2.2 Animal Preparation

Mice (CD-1, male, 25-30 g, Charles River) were anesthetized with medical air vaporized isoflurane (2%) via nose-cone inhalation. Body temperature was maintained at 37 °C with a feedback heating pad (DC Temperature Controller, Future Health Concepts). Arterial oxygen saturation, heart rate, and breath rate were monitored via pulse oximetry (MouseOx, Starr Life Sciences). After induction, mice were placed supine in a stereotaxic frame (Narishige Scientific Instrument Lab) and administered carprofen (5 mg/kg, subcutaneous) and dexamethasone (2 mg/kg, intramuscular) to reduce inflammation of the brain during the craniotomy procedure. The scalp was shaved and resected to expose skull between the bregma and lambda cranial coordinates. A thin layer of cyanoacrylate (Vetbond Tissue Adhesive, 3M) was applied to the exposed skull to facilitate the adhesion of dental cement during a later step. A 3 mm diameter portion of the skull over the frontoparietal cortex was removed with a dental drill (Ideal Microdrill, 0.8 mm burr, Fine Science Tools) while leaving the dura intact. The craniotomy was performed under regular perfusion of artificial cerebrospinal fluid to protect the brain from overheating. A 5 mm round cover glass (#1.5, World Precision Instruments) was placed over the exposed brain and a dental cement mixture was deposited along the perimeter, bonding it to the surrounding skull. This process created a sterile, air-tight seal around the craniotomy and allowed for restoration of intracranial pressure. A layer of

cyanoacrylate was applied over the dental cement to further seal the cranial window. The medial and anterior edges of the window were approximately 2 mm rostral to bregma and 0.5 mm lateral to midline. Animals were allowed to recover from anesthesia and monitored for cranial window integrity and normal behavior for two weeks prior to imaging. All imaging sessions were conducted using medical air with 1.5% vaporized isoflurane. The Institutional Animal Care and Use Committee at The University of Texas at Austin approved of all experiments.

2.3 Laser Speckle Contrast Image Analysis

The raw images captured by the camera were converted to speckle contrast images using Eq. (1), where speckle contrast (K) is defined as the ratio of the standard deviation (σ_s) to the mean intensity ($\langle I \rangle$) within a small region of the image. The full speckle contrast image was calculated using a 7x7-pixel sliding window centered at every pixel of the raw image and was computed, displayed, and saved in real-time using an efficient processing algorithm.[21]

$$K = \frac{\sigma_s}{\langle I \rangle} \tag{1}$$

During post-processing, speckle contrast images were averaged together ($n = 45$) and converted to inverse correlation time ($1/\tau_c$) images to provide a more quantitative measure of blood flow.[1] The observed speckle contrast (K) was fitted for its corresponding correlation time (τ_c) at each pixel using Eq. (2), where $x = T/\tau_c$.[22] T is the camera exposure duration (5 ms) and β is an instrumentation factor that accounts for speckle sampling, polarization, and coherence effects.

$$K(T, \tau_c) = \left(\beta \frac{e^{-2x} - 1 + 2x}{2x^2} \right)^{1/2} \tag{2}$$

Each inverse correlation time image was then baselined against the first frame to calculate an estimate of relative change in blood flow ($rCFB = \tau_{c,initial}/\tau_c$).[23] Because β is a property of the instrumentation and should not vary throughout the course of an experiment, it was assumed $\beta = 1$. The same regions of interest defined for DMD structured illumination were used to calculate timecourses of the relative change in flow.

2.4 Oxygen Tension Measurements

Oxyphor PtG4 is an oxygen-sensitive dendritic probe that contains Platinum(II)-meso-tetra-(3,5-dicarboxyphenyl)tetrabenzoporphyrin as the phosphorescent core[19,24] and has been effectively used to measure absolute oxygen tension using phosphorescence quenching.[25,26] It has two excitation maxima near 435 nm and 623 nm and an emission maximum at 782 nm (Fig. 2a). Unlike previous generations of the Oxyphor probe, PtG4 is highly soluble in an aqueous environment without requiring the presence of environmental albumin for stabilization.[19] For *in vivo* measurements, Oxyphor PtG4 was introduced systemically via retro-orbital injection into the venous sinus for a target blood plasma concentration of 5 μM. Phosphorescence lifetime measurements were made in the time domain using the structured pulsed excitation light paradigm described above. The instrument response was accounted for by introducing a 2 μs temporal offset to the phosphorescent signal [$I(t)$] prior to fitting for the decay lifetime (τ) in Eq. (3).

$$I(t) = A + Be^{-t/\tau} \tag{3}$$

A calibration curve based on Stern-Volmer kinetics[27,28] was used to convert the measured lifetime (τ) to the absolute pO_2. The calibration of Oxyphor PtG4 under physiological conditions is

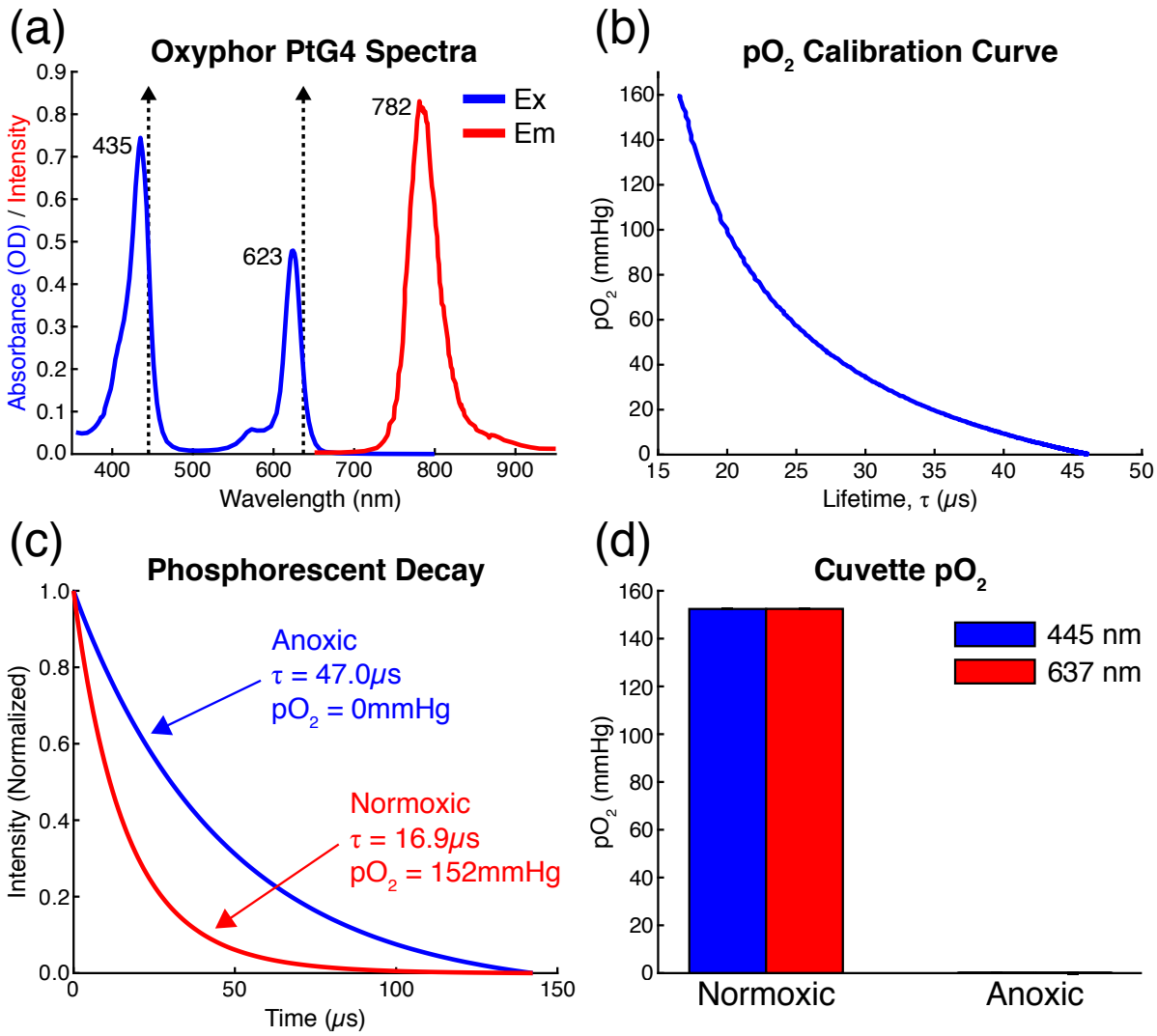

Fig 2 (a) Excitation and emission spectra for Oxyphor PtG4. Dashed vertical lines indicate excitation lasers at 445 nm and 637 nm. (b) Calibration curve relating pO_2 to the measured phosphorescence lifetime (τ) under physiological conditions (37 °C, pH 7.2). For $\tau < 16$ μs, Stern-Volmer kinetics were assumed with $k_q = 291.014$ mmHg^{-1} s^{-1} and $\tau_0 = 47$ μs. (c) Averaged phosphorescent decay curves ($n = 200$) in anoxic and normoxic cuvette environments with fitted lifetimes and their corresponding pO_2 values. (d) Excitation wavelength does not affect measured pO_2.

shown in Fig. 2b. The unquenched lifetime is 47 μs in an oxygen-free environment. Fig. 2c depicts phosphorescent decay curves and their corresponding pO_2 values within anoxic and normoxic cuvette environments with 10 μM Oxyphor PtG4. Anoxia was established using the enzymatic reaction between glucose and glucose oxidase to scavenge oxygen from a sealed cuvette.[29] Lifetime measurements in cuvette samples did not vary with excitation wavelength (Fig. 2d).

2.5 *Hyperoxic Challenge*

Detection of systemic changes in oxygen tension was demonstrated by subjecting mice to a hyperoxic challenge. The oxygen fraction of inspired air under anesthesia was increased from 21% (normoxia) to 100% and then decreased back to normoxia for recovery. Hyperoxia was maintained for five minutes and vascular pO_2 measurements were acquired at the end of each stage. Pulse oximetry was used to monitor the status of the animal throughout the hyperoxic challenge.

2.6 *Targeted Photothrombosis*

The DMD was also used to induce arbitrarily-shaped photothrombotic occlusions in the cortical vasculature using rose bengal. Rose bengal is a fast-clearing photothrombotic agent that photochemically triggers localized clot formation upon irradiation with green light.[30–32] Structured illumination with the DMD allows for the selective targeting of individual vessels for occlusion while minimizing exposure in the surrounding parenchyma. Rose bengal was injected intravenously (50 μL, 15 mg/mL) and the target vessels exposed to DMD-patterned 532 nm laser light for 5 - 10 minutes. Descending arterioles were the primary targets because they serve as bottlenecks in the cortical oxygen supply.[33] Oxygen tension measurements were restricted when performing photothrombosis to the region being targeted for occlusion. LSCI was used to monitor clot formation within the targeted area and control the progression of the occlusion.

3 Results

3.1 *Excitation Wavelength Dependence of Measured Oxygen Tension*

Static oxygen tension measurements in the vasculature of the mouse cortex are shown in Fig. 3. Five different regions including two arterioles, two veins, and an area of unresolvable vasculature

(parenchyma) were targeted for selective illumination using both the 445 nm and 637 nm excitation lasers (Fig. 3a). The measured pO_2 within each region aligns well with physiological expectations as both arterioles have higher pO_2 than the venous or parenchymal areas (Fig. 3b). The effects of wavelength can be seen as 445 nm excitation resulted in a broader range of oxygen tension values (48 - 83 mmHg) compared to 637 nm excitation (75 - 82 mmHg). Despite differences in absolute value, similar trends exist between each of the targeted regions for both excitation wavelengths. As shown previously in Fig. 2d, no differences in pO_2 were observed between the two wavelengths in cuvette samples.

In order to obtain a more comprehensive look at vascular oxygenation within the LSCI field of view, an array of 12x8 rectangular tiles was sequentially projected. The tiles were displayed at 10 Hz with 200 decays averaged per pattern for a total acquisition time of 9.6 seconds. The resulting pO_2 maps (Fig. 3c, d) coarsely follow the visible surface vasculature. As expected, the large branching vein has lower pO_2 values compared to the arteriole approaching from the bottom or the surrounding parenchyma. 445 nm excitation again resulted in a wider range of pO_2 values (45 - 85 mmHg) compared to 637 nm excitation (81 - 85 mmHg).

3.2 Hyperoxic Challenge

The ability to detect changes in neurovascular oxygen tension was tested using an hyperoxic challenge as shown in Fig. 4. Three regions covering an arteriole, venule, and parenchyma were targeted for selective 445 nm illumination (Fig. 4a) as the oxygen fraction was temporarily increased. Measurements were taken during each stage of the challenge and detected a large increase in pO_2 during the hyperoxic state across all three regions (Fig. 4b) with the arteriole experiencing the largest net increase. The pO_2 remained slightly elevated above baseline values several minutes

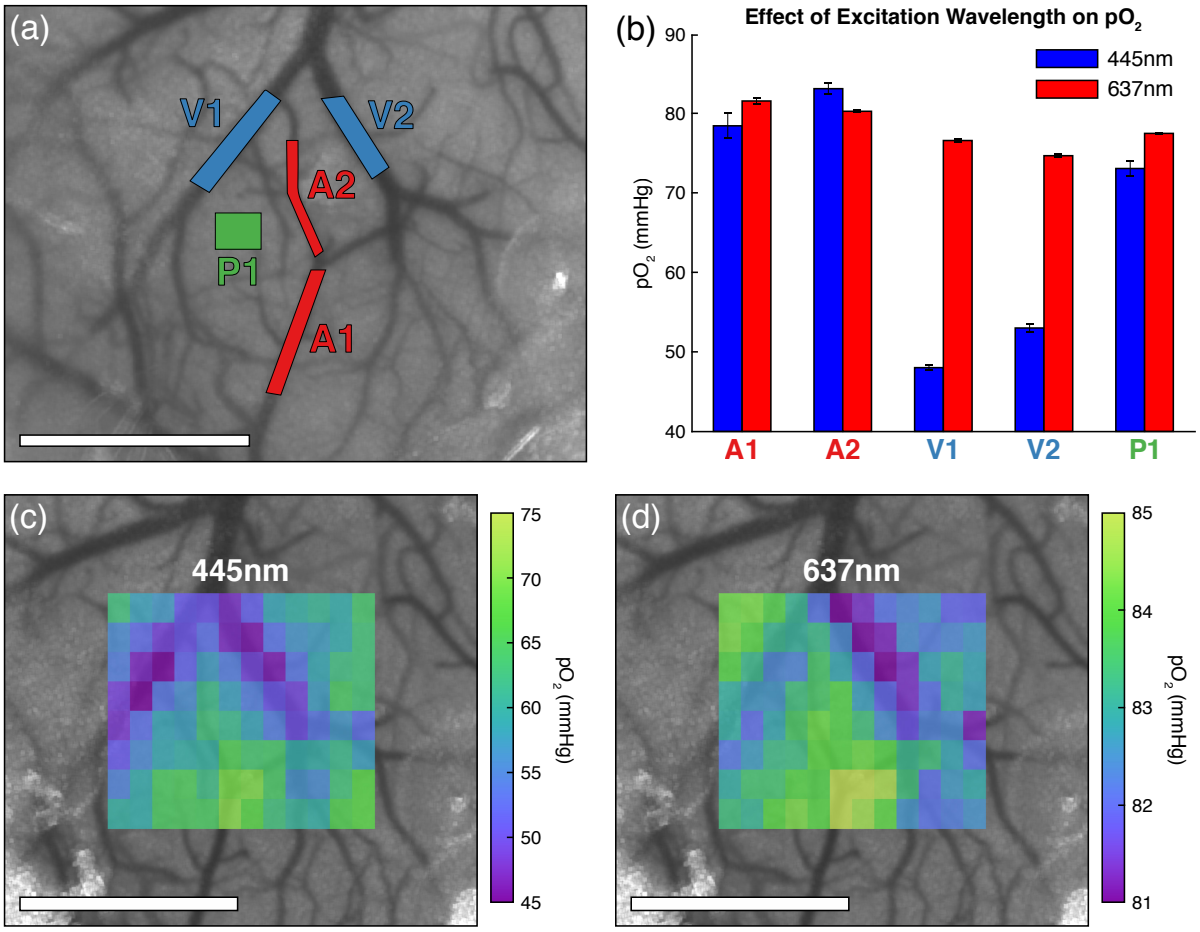

Fig 3 Scale bars = 1 mm. (a) Speckle contrast image of cortical flow overlaid with regions targeted for pO_2 measurements. Two descending arterioles (A1, A2), two veins (V1, V2), and one parenchyma region (P1) were examined. The projected patterns ranged between 0.014 - 0.046 mm^2 in area. (b) pO_2 measurements within the targeted regions conducted using both 445 nm and 637 nm excitation of Oxyphor PtG4 (mean $\pm$ s.d.). (c) 445 nm and (d) 637 nm pO_2 maps produced using tiled excitation patterns covering a 1.2 x 1.0 mm area. Each individual tile has a projected area of 0.012 mm^2.

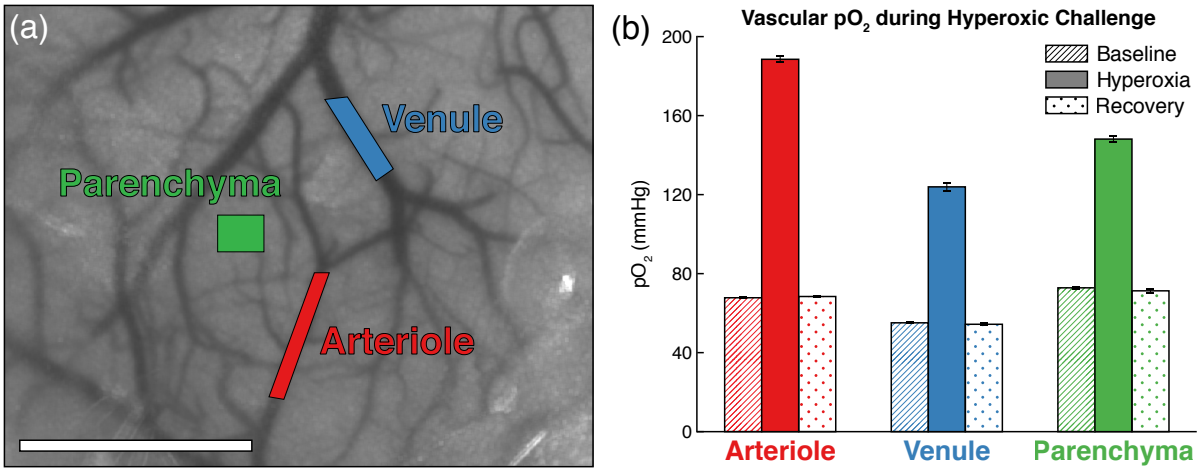

Fig 4 Scale bar = 1 mm. (a) Speckle contrast image depicting three regions (arteriole, venule, and parenchyma) targeted for 445 nm pO_2 measurements during an hyperoxic challenge. (b) Static pO_2 during baseline, hyperoxic, and recovery stages for each of the targeted vessels (mean $\pm$ s.d.).

later during the post-hyperoxia recovery stage.

3.3 Oxygen Tension and Blood Flow during Photothrombosis

Targeted photothrombosis within a descending arteriole can be seen in the series of speckle contrast images in Fig. 5a. The red overlay in the first frame depicts the 0.09 mm^2 region illuminated with DMD-targeted 532 nm light for 420 seconds. Because Oxyphor PtG4 has minimal absorbance of green light (Fig. 2a), pO_2 measurements using 445 nm excitation were simultaneously acquired from the same region. The remaining frames depict the progression of the photothrombotic occlusion as the targeted vessel underwent stenosis and flow was significantly reduced. After two minutes of exposure, the occluded area was indistinguishable from the surrounding parenchyma.

Fig. 5b depicts the five regions targeted for continuous relative blood flow and 445 nm pO_2 measurements. The first arteriole region (A1) is the same vessel targeted for photothrombotic occlusion. The resulting timecourses of relative blood flow and pO_2 within each region can be seen in Fig. 5c. By $t = 120$ s, relative flow within the targeted arteriole decreased to $<50\%$ of

baseline and pO_2 fell from 80 mmHg to only 20 mmHg. The propagation of an ischemia-induced depolarization event[34,35] can be seen beginning at $t = 300$ s with sharp reductions in both relative flow and pO_2. As the depolarization subsided, flow within the targeted arteriole further decreased to $<35\%$ of baseline while the pO_2 returned to pre-depolarization levels around 20 mmHg.

Both relative blood flow and pO_2 decreased over the remainder of the imaging session across all regions but the targeted arteriole. At $t = 860$ s, the vessel partially reperfused, causing a sudden increase in both relative blood flow (+6 percentage points) and pO_2 (+15 mmHg). By the end of the imaging session, relative blood flow had increased to 55% of baseline and pO_2 to 42 mmHg, likely indicating further reperfusion of the vessel.

3.4 Chronic Imaging of Oxygen Tension and Blood Flow

The chronic progression of the ischemia was tracked for eight days following photothrombosis. The perfusion of the occluded arteriole and broader effect on cortical flow was tracked using LSCI as shown in Fig. 6a. Tiled pO_2 maps acquired using both 445 nm and 637 nm excitation reveal the spatial extent of the oxygen deficit (Fig. 6b, c). The same five regions used during photothrombosis were targeted for chronic relative blood flow and pO_2 measurements (Fig. 6d-f). Relative blood flow was calculated using the pre-stroke (Day -0) measurements as baseline.

The first post-stroke measurements (Day +0) were taken immediately after the induction of photothrombosis and revealed global deficits in both blood flow and pO_2. Over the next two days, the targeted arteriole partially reperfused and the infarct was localized to the surrounding area. By Day +5, the vessel had fully reperfused and pO_2 measurements returned to near baseline levels.

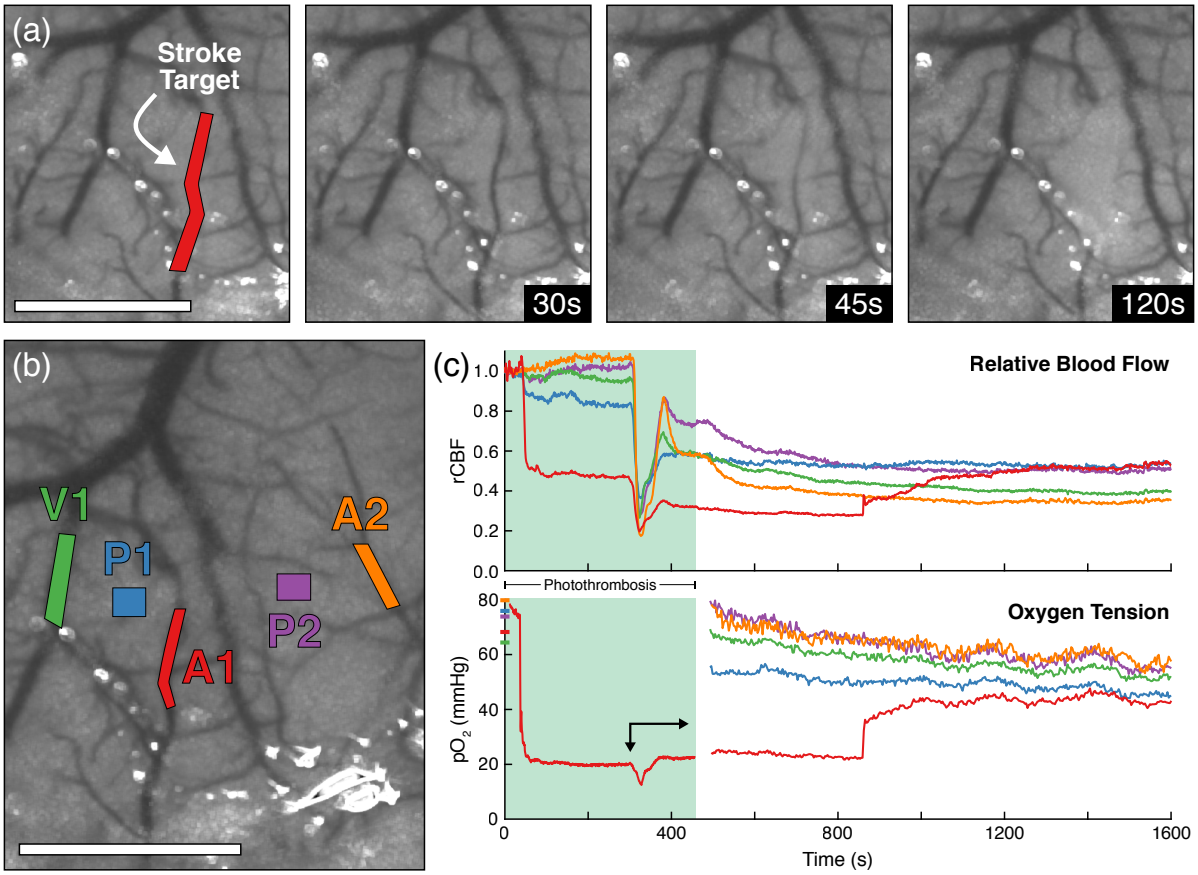

Fig 5 Scale bars = 1 mm. (a) Speckle contrast images depicting the occlusion of a descending arteriole using DMD-targeted photothrombosis (Video 1, MPEG4, 26.9 MB). The red overlay indicates the 0.09 mm^2 region simultaneously illuminated for occlusion and pO_2 measurements. (b) Two arterioles (A1, A2), one vein (V1), and two parenchyma regions (P1, P2) were targeted for pO_2 measurements after stroke induction. (c) Relative blood flow and pO_2 within the targeted regions during and after photothrombosis. The green-shaded section indicates irradiation of the targeted arteriole. The arrow indicates the propagation of an ischemia-induced depolarization event.

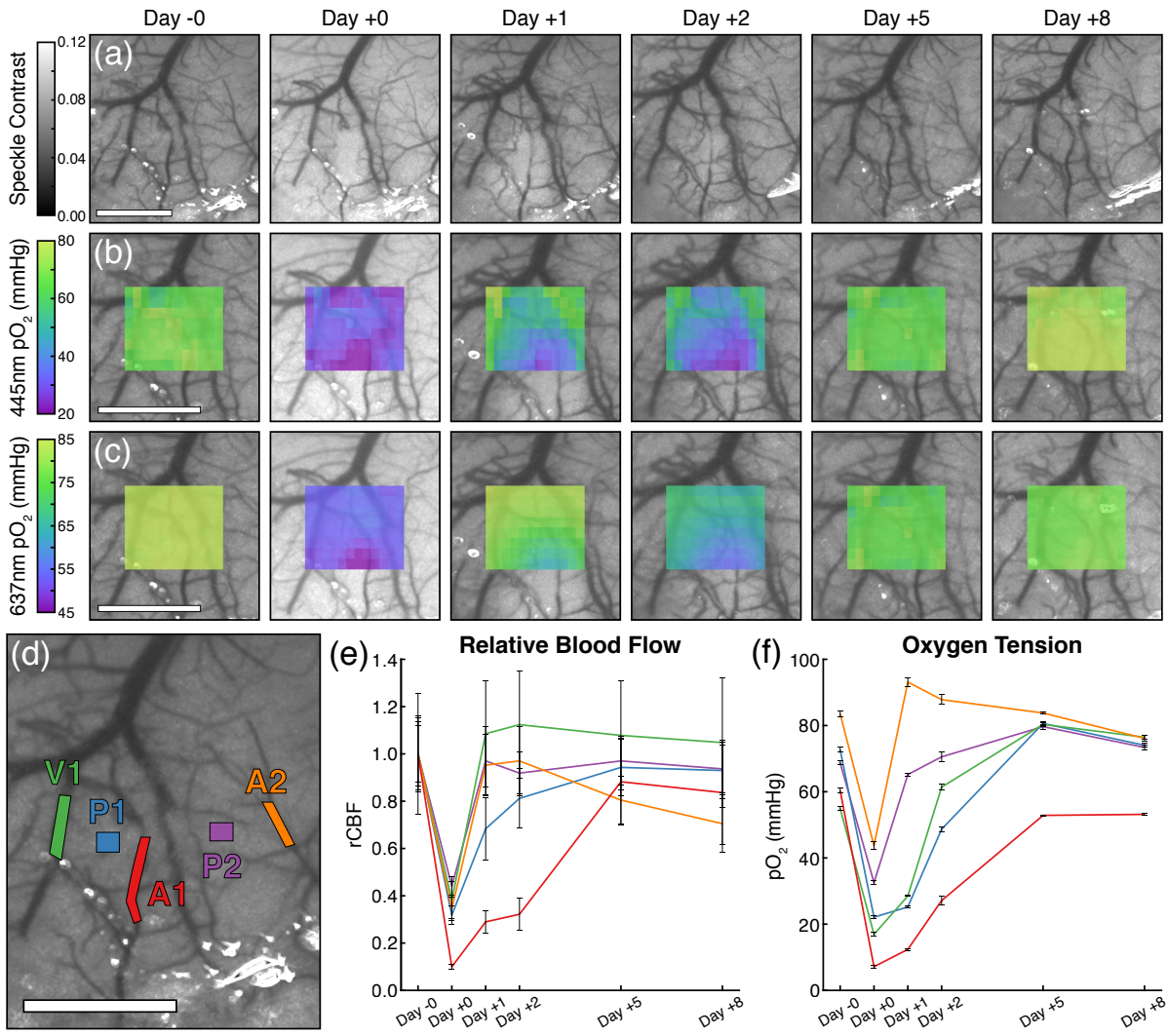

Fig 6 Scale bars = 1 mm. Progression of the ischemic lesion over eight days as imaged with (a) LSCI, (b) 445 nm tiled pO_2, and (c) 637 nm tiled pO_2 measurements. Day -0 measurements were taken immediately prior to photothrombosis induction and Day +0 measurements were taken immediately after. (d) Two arterioles (A1, A2), one vein (V1), and two parenchyma regions (P1, P2) were targeted for chronic (e) relative blood flow and (f) 445 nm pO_2 measurements (mean $\pm$ s.d.). The relative blood flow was baselined against Day -0 measurements.

4 Discussion

The combination of laser speckle contrast imaging and phosphorescence lifetime imaging is a purely optical, non-contact strategy for measuring blood flow and oxygen tension within the cortex. This system builds upon prior work that used structured illumination to overcome traditional limitations of lifetime imaging.[18] Spatially patterning excitation light with a DMD allows for the use of a point detector, which offers both high sensitivity and speed for the collection of the phosphorescent signal. The spatial and temporal resolutions of the system are ultimately limited by noise. Regions as small as 0.01 mm^2 can reliably be excited at a pattern repetition rate of 10 Hz with 200 phosphorescent decays collected and averaged per pattern. Because intensity of the excitation light scales with the size of the target area, larger regions could allow for faster pattern rates at the expense of averaging (e.g. 100 Hz with 20-decay averaging). However, a 10 Hz pattern rate is more than sufficient for visualizing dynamic physiological events such as spreading depolarizations, which have been reported to propagate at a rate of several millimeters per minute.[36]

The comparison of excitation wavelengths revealed significant differences in measured oxygen tension. Static pO_2 measurements under 445 nm illumination spanned a range five times larger than that of 637 nm illumination. This discrepancy was most noticeable in venous regions, with the shorter excitation wavelength resulting in pO_2 values around 50 mmHg whereas the longer wavelength resulted in values around 75 mmHg. Since depth penetration is heavily dependent upon wavelength,[37] the difference is likely the result of photons sampling a much larger volume of tissue under 637 nm illumination. An estimate of transmission through a surface vessel at both wavelengths can be obtained using the Beer-Lambert Law. Because scattering increases the distance traveled by photons in tissue, this represents the most conservative estimate of the effect

of wavelength on transmission. Assuming hemoglobin is the primary absorber in blood plasma with a concentration of 2.3 mM[38] and 95% SaO_2, the transmittance at 445 nm and 637 nm through a 100 μm arteriole is 0.9% and 96.5%, respectively. As excitation wavelength approaches the tissue optical window, the transmission of incident light significantly increases. The 445 nm light is almost entirely confined within a vessel of that caliber and does not extensively sample deeper microvasculature. Because the 637 nm light penetrates further into the brain, the measured pO_2 is skewed away from the vascular value and is more representative of a bulk volumetric average. This is consistent with prior Monte Carlo modeling that found fluorescence primarily originates from within surface vasculature at shorter wavelengths.[20]

The creation of an extended occlusion within an arteriole using targeted photothrombosis was demonstrated for the first time. Previous methods relied upon broad illumination to occlude a large volume of vasculature[30] or highly focused light to occlude a single part of a microvessel.[39] The previous iteration of this system could only induce occlusions within a large region and pO_2 measurements could not be simultaneously acquired.[18] While photothrombosis is widely utilized, there is evidence it does not produce pathophysiologically relevant ischemic lesions.[40] This system allows for greater control over the spatial characteristics of the stroke (e.g. size and location) and the option to target the entirety of individual vessels or even multiple vessels simultaneously.

While tissue pO_2 during ischemic depolarizations has been previously examined,[41] to our knowledge no studies have quantified the acute vascular response to a depolarization event or the chronic response to an ischemic infarct. The depolarization results in a global flow reduction across all regions, which is consistent with previous reports using other stroke models.[34,42] Within the targeted arteriole, the blood flow reduction is of greater magnitude (-58%) than the corresponding decrease in pO_2 (-44%), which eventually recovers to slightly above pre-depolarization levels.

Unfortunately it is difficult to predict how the pO_2 responded to the depolarization across the other regions, but it likely mirrored the LSCI results.

The chronic measurements revealed a severe post-stroke blood flow and oxygen deficit that recovered almost completely within five days. The spatial extent of the ischemia can be clearly seen on Days +1 and +2 in both the speckle contrast imagery and tiled pO_2 maps. The large gradient between the occluded vessel and surrounding tissue resembles the ischemic penumbra that the photothrombotic technique rarely produces.[40] By Day +5, the targeted vessel appeared to have fully reperfused and there was no evidence of hypoxia in the tiled pO_2 measurements. The speed of this recovery is faster than previously reported,[43] but can likely be explained by the smaller area targeted for photothrombosis, which resulted in a less severe ischemic lesion.

4.1 Limitations

A potential concern for this system is the scattering of light beyond the desired region of interest when performing the pO_2 measurements or targeted photothrombosis. This problem is highlighted by the discrepancies seen in pO_2 values under 445 nm and 637 nm illumination and introduces the risk of collateral tissue damage. The wavelength dependence of light propagation also means the LSCI and pO_2 measurements sample different volumes of tissue. The use of anesthesia during imaging significantly affects systemic hemodynamics[44] and has been shown to inhibit the oxygen autoregulatory response.[45] The implementation of an awake imaging setup[46] would resolve this issue by completely eliminating the need for anesthesia during imaging. Another concern is that estimates of blood flow provided by single-exposure speckle imaging have limitations for chronic imaging or cross-animal comparisons.[47] An enhanced technique known as Multi-Exposure Speckle Imaging (MESI) has been developed to increase the quantitative accuracy of flow mea-

surements.[48] Implementing MESI would allow for more robust chronic measurements of blood flow in the ischemic brain.

5 Conclusion

We have presented an imaging system capable of simultaneously measuring relative cerebral blood flow and vascular oxygen tension at higher spatiotemporal resolutions than its predecessor. We demonstrated the ability to perform targeted pO_2 measurements *in vivo* using both 445 nm and 637 nm illumination. The discrepancy in pO_2 values between the two wavelengths highlighted the influence of penetration depth on single-photon phosphorescence measurements. We also demonstrated the induction of a DMD-targeted photothrombotic stroke within a single vessel and imaged blood flow and oxygen tension during a subsequent ischemic depolarization. Chronic imaging revealed a rapid recovery, with the occluded vessel fully reperfusing and the pO_2 returning to baseline levels within only five days. This system will have broad applications for studying the progression of ischemic stroke and other vascular pathologies in the brain.

Disclosures

No conflicts of interest, financial or otherwise, are declared by the authors.

Acknowledgments

This study was supported by the National Institutes of Health (EB011556, NS078791, NS082518) and the American Heart Association (14EIA8970041).

References

1 J. D. Briers, "Laser Doppler, speckle and related techniques for blood perfusion mapping and imaging," *Physiological Measurement* **22**, R35–R66 (2001).

2 A. K. Dunn, H. Bolay, M. A. Moskowitz, *et al.*, "Dynamic imaging of cerebral blood flow using laser speckle," *Journal of Cerebral Blood Flow & Metabolism* **21**, 195–201 (2001).

3 D. A. Boas and A. K. Dunn, "Laser speckle contrast imaging in biomedical optics," *Journal of Biomedical Optics* **15**, 011109–011109–12 (2010).

4 A. K. Dunn, "Laser Speckle Contrast Imaging of Cerebral Blood Flow," *Annals of Biomedical Engineering* **40**, 367–377 (2011).

5 E. Vovenko, "Distribution of oxygen tension on the surface of arterioles, capillaries and venules of brain cortex and in tissue in normoxia: an experimental study on rats," *Pflügers Archiv: European Journal of Physiology* **437**(4), 617–623 (1999).

6 A. G. Tsai, P. C. Johnson, and M. Intaglietta, "Oxygen gradients in the microcirculation," *Physiological Reviews* **83**, 933–963 (2003).

7 E. Roussakis, Z. Li, A. J. Nichols, *et al.*, "Oxygen-Sensing Methods in Biomedicine from the Macroscale to the Microscale," *Angewandte Chemie International Edition* **54**, 8340–8362 (2015).

8 J. F. Dunn and H. M. Swartz, "In vivo electron paramagnetic resonance oximetry with particulate materials," *Methods* **30**, 159–166 (2003).

9 S. Liu, H. Shi, W. Liu, *et al.*, "Interstitial pO_2 in Ischemic Penumbra and Core are Differentially Affected Following Transient Focal Cerebral Ischemia in Rats," *Journal of Cerebral Blood Flow & Metabolism* **24**, 343–349 (2004).

10 H. Hou, O. Y. Grinberg, S. Taie, *et al.*, "Electron paramagnetic resonance assessment of brain tissue oxygen tension in anesthetized rats," *Anesthesia Analgesia* **96**, 1467–1472 (2003).

11 S. Liu, W. Liu, W. Ding, *et al.*, "Electron paramagnetic resonance-guided normobaric hyperoxia treatment protects the brain by maintaining penumbral oxygenation in a rat model of transient focal cerebral ischemia," *Journal of Cerebral Blood Flow & Metabolism* **26**, 1274–1284 (2006).

12 S. A. Vinogradov and D. F. Wilson, "Porphyrin dendrimers as biological oxygen sensors," in *Designing Dendrimers*, S. Campagna, P. Ceroni, and F. Puntoriero, Eds., 463–504, Wiley, New York (2012).

13 R. D. Shonat and A. C. Kight, "Oxygen Tension Imaging in the Mouse Retina," *Annals of Biomedical Engineering* **31**, 1084–1096 (2003).

14 S. Sakadžić, S. Yuan, E. Dilekoz, *et al.*, "Simultaneous imaging of cerebral partial pressure of oxygen and blood flow during functional activation and cortical spreading depression," *Applied Optics* **48**, D169–D177 (2009).

15 M. A. Yaseen, V. J. Srinivasan, S. Sakadžić, *et al.*, "Optical monitoring of oxygen tension in cortical microvessels with confocal microscopy.," *Optics Express* **17**, 22341–22350 (2009).

16 S. M. S. Kazmi, S. A. Vinogradov, A. J. Salvaggio, *et al.*, "Three-dimensional mapping of oxygen tension in cortical arterioles before and after occlusion," *Biomedical Optics Express* **4**, 1061–1073 (2013).

17 A. Devor, S. Sakadžić, M. A. Yaseen, *et al.*, "Functional Imaging of Cerebral Oxygenation with Intrinsic Optical Contrast and Phosphorescent Probes," in *Optical Imaging of Neocortical Dynamics*, B. Weber and F. Helmchen, Eds., 225–253, Humana Press, New York (2014).

18 A. Ponticorvo and A. K. Dunn, "Simultaneous imaging of oxygen tension and blood flow in animals using a digital micromirror device," *Optics Express* **18**, 8160–8170 (2010).

19 T. V. Esipova, A. Karagodov, J. Miller, *et al.*, "Two New "Protected" Oxyphors for Biological Oximetry: Properties and Application in Tumor Imaging," *Analytical Chemistry* **83**(22), 8756–8765 (2011).

20 M. A. Davis, S. M. S. Kazmi, A. Ponticorvo, *et al.*, "Depth dependence of vascular fluorescence imaging," *Biomedical Optics Express* **2**, 3349–3362 (2011).

21 W. J. Tom, A. Ponticorvo, and A. K. Dunn, "Efficient processing of laser speckle contrast images," *IEEE Transactions on Medical Imaging* **27**(12), 1728–1738 (2008).

22 R. Bandyopadhyay, A. S. Gittings, S. S. Suh, *et al.*, "Speckle-visibility spectroscopy: A tool to study time-varying dynamics," *Review of Scientific Instruments* **76**, 093110 (2005).

23 S. M. S. Kazmi, E. Faraji, M. A. Davis, *et al.*, "Flux or speed? Examining speckle contrast imaging of vascular flows," *Biomedical Optics Express* **6**, 2588–2608 (2015).

24 A. Y. Lebedev, A. V. Cheprakov, S. Sakadžić, *et al.*, "Dendritic Phosphorescent Probes for Oxygen Imaging in Biological Systems," *ACS Applied Materials & Interfaces* **1**, 1292–1304 (2009).

25 R. Zhang, S. C. Davis, J.-L. H. Demers, *et al.*, "Oxygen tomography by Čerenkov-excited phosphorescence during external beam irradiation," *Journal of Biomedical Optics* **18**, 050503–050503 (2013).

26 R. W. Holt, R. Zhang, R. Zhang, *et al.*, "Cherenkov excited phosphorescence-based pO2 estimation during multi-beam radiation therapy: phantom and simulation studies," *Physics in Medicine and Biology* **59**, 5317–5328 (2014).

27 J. M. Vanderkooi and D. F. Wilson, "A New Method for Measuring Oxygen Concentration in Biological Systems," in *Oxygen Transport to Tissue VIII*, I. S. Longmuir, Ed., 189–193, Advances in Experimental Medicine and Biology, Boston, MA (1986).

28 D. F. Wilson, S. A. Vinogradov, P. Grosul, *et al.*, "Oxygen Distributions in Tissue Measured by Phosphorescence Quenching," in *Oxygen Transport To Tissue XXIII*, D. F. Wilson, S. M. Evans, J. Biaglow, *et al.*, Eds., 181–185, Springer US, Boston, MA (2003).

29 L.-W. Lo, S. A. Vinogradov, C. J. Koch, *et al.*, "A New, Water Soluble, Phosphor for Oxygen Measurements *In Vivo*," in *Oxygen Transport to Tissue XIX*, D. K. Harrison and D. T. Delpy, Eds., 651–656, Springer US, Boston, MA (1997).

30 B. D. Watson, W. D. Dietrich, R. Busto, *et al.*, "Induction of reproducible brain infarction by photochemically initiated thrombosis," *Annals of Neurology* **17**, 497–504 (1985).

31 C. D. Klaassen, "Pharmacokinetics of rose bengal in the rat, rabbit, dog, and guinea pig," *Toxicology and Applied Pharmacology* **38**, 85–100 (1976).

32 C. A. Wilson and D. L. Hatchell, "Photodynamic Retinal Vascular Thrombosis - Rate and Duration of Vascular Occlusion," *Investigative Ophthalmology & Visual Science* **32**, 2357–2365 (1991).

33 N. Nishimura, C. B. Schaffer, B. Friedman, *et al.*, "Penetrating arterioles are a bottleneck in the perfusion of neocortex," *Proceedings of the National Academy of Sciences of the United States of America* **104**, 365–370 (2007).

34 H. K. Shin, A. K. Dunn, P. B. Jones, *et al.*, "Vasoconstrictive neurovascular coupling during focal ischemic depolarizations," *Journal of Cerebral Blood Flow & Metabolism* **26**, 1018–1030 (2006).

403 35 J. P. Dreier, "The role of spreading depression, spreading depolarization and spreading is-
404 chemia in neurological disease," *Nature Medicine* **17**, 439–447 (2011).
405 36 M. Lauritzen, "Pathophysiology of the migraine aura. The spreading depression theory,"
406 *Brain* **117**, 199–210 (1994).
407 37 X. Deng and M. Gu, "Penetration depth of single-, two-, and three-photon fluorescence mi-
408 croscopic imaging through human cortex structures: Monte Carlo simulation," *Applied Op-*
409 *tics* **42**, 3321–3329 (2003).
410 38 F. E. Robles, S. Chowdhury, and A. Wax, "Assessing hemoglobin concentration using spec-
411 troscopic optical coherence tomography for feasibility of tissue diagnostics," *Biomedical Op-*
412 *tics Express* **1**(1), 310–317 (2010).
413 39 C. B. Schaffer, B. Friedman, N. Nishimura, *et al.*, "Two-Photon Imaging of Cortical Surface
414 Microvessels Reveals a Robust Redistribution in Blood Flow after Vascular Occlusion," *PLoS*
415 *Biology* **4**, e22 (2006).
416 40 S. T. Carmichael, "Rodent Models of Focal Stroke: Size, Mechanism, and Purpose," *NeuroRX*
417 **2**, 396–409 (2005).
418 41 D. von Bornstädt, T. Houben, J. L. Seidel, *et al.*, "Supply-Demand Mismatch Transients in
419 Susceptible Peri-infarct Hot Zones Explain the Origins of Spreading Injury Depolarizations,"
420 *Neuron* **85**, 1117–1131 (2015).
421 42 H. Nakamura, A. J. Strong, C. Dohmen, *et al.*, "Spreading depolarizations cycle around and
422 enlarge focal ischaemic brain lesions," *Brain* **133**, 1994–2006 (2010).
423 43 C. J. Schrandt, S. M. S. Kazmi, T. A. Jones, *et al.*, "Chronic monitoring of vascular progres-

sion after ischemic stroke using multiexposure speckle imaging and two-photon fluorescence microscopy.," *Journal of Cerebral Blood Flow & Metabolism* (2015).

44 B. J. A. Janssen, T. De Celle, J. J. M. Debets, *et al.*, "Effects of anesthetics on systemic hemodynamics in mice," *American Journal of Physiology - Heart and Circulatory Physiology* **287**, H1618–H1624 (2004).

45 D. Aksenov, J. E. Eassa, J. Lakhoo, *et al.*, "Effect of isoflurane on brain tissue oxygen tension and cerebral autoregulation in rabbits," *Neuroscience Letters* **524**, 116–118 (2012).

46 D. A. Dombeck, A. N. Khabbaz, F. Collman, *et al.*, "Imaging large-scale neural activity with cellular resolution in awake, mobile mice," *Neuron* **56**, 43–57 (2007).

47 S. M. S. Kazmi, A. B. Parthasarathy, N. E. Song, *et al.*, "Chronic imaging of cortical blood flow using Multi-Exposure Speckle Imaging," *Journal of Cerebral Blood Flow & Metabolism* **33**, 798–808 (2013).

48 A. B. Parthasarathy, W. J. Tom, A. Gopal, *et al.*, "Robust flow measurement with multi-exposure speckle imaging," *Optics Express* **16**, 1975–1989 (2008).

Colin T. Sullender received his B.S. in Bioengineering from the University of Washington in 2011 and his M.S.E. in Biomedical Engineering from the University of Texas at Austin in 2016. He is currently a doctoral candidate in the Department of Biomedical Engineering at the University of Texas at Austin working in Dr. Andrew Dunn's Functional Optical Imaging Laboratory.

Taylor A. Clark received her B.S. in Psychology from the University of California, Los Angeles in 2013. She is currently a doctoral candidate in the Department of Neuroscience at the University of Texas at Austin working in Dr. Theresa Jones' behavioral neuroscience laboratory.

Theresa A. Jones is a professor in the Department of Psychology at the University of Texas at Austin. Her research focuses on the plasticity of neural structure and synaptic connectivity following brain damage and during skill learning.

Andrew K. Dunn is the Donald J. Douglass Centennial Professor of Engineering in the Department of Biomedical Engineering at the University of Texas at Austin. His research focuses on the development of novel optical imaging techniques for studying the brain.

Biographies of the other authors and photographs are not available.

List of Figures

2 (a) Excitation and emission spectra for Oxyphor PtG4. Dashed vertical lines indicate excitation lasers at 445 nm and 637 nm. (b) Calibration curve relating pO_2 to the measured phosphorescence lifetime (τ) under physiological conditions (37 °C, pH 7.2). For $\tau < 16$ μs, Stern-Volmer kinetics were assumed with $k_q = 291.014$ mmHg^{-1} s^{-1} and $\tau_0 = 47$ μs. (c) Averaged phosphorescent decay curves ($n = 200$) in anoxic and normoxic cuvette environments with fitted lifetimes and their corresponding pO_2 values. (d) Excitation wavelength does not affect measured pO_2.

3 Scale bars = 1 mm. (a) Speckle contrast image of cortical flow overlaid with regions targeted for pO_2 measurements. Two descending arterioles (A1, A2), two veins (V1, V2), and one parenchyma region (P1) were examined. The projected patterns ranged between 0.014 - 0.046 mm^2 in area. (b) pO_2 measurements within the targeted regions conducted using both 445 nm and 637 nm excitation of Oxyphor PtG4 (mean $\pm$ s.d.). (c) 445 nm and (d) 637 nm pO_2 maps produced using tiled excitation patterns covering a 1.2 x 1.0 mm area. Each individual tile has a projected area of 0.012 mm^2.

4 Scale bar = 1 mm. (a) Speckle contrast image depicting three regions (arteriole, venule, and parenchyma) targeted for 445 nm pO_2 measurements during an hyperoxic challenge. (b) Static pO_2 during baseline, hyperoxic, and recovery stages for each of the targeted vessels (mean $\pm$ s.d.).

480 5 Scale bars = 1 mm. (a) Speckle contrast images depicting the occlusion of a de-
481 scending arteriole using DMD-targeted photothrombosis (Video 1, MPEG4, 26.9
482 MB). The red overlay indicates the 0.09 mm^2 region simultaneously illuminated
483 for occlusion and pO_2 measurements. (b) Two arterioles (A1, A2), one vein (V1),
484 and two parenchyma regions (P1, P2) were targeted for pO_2 measurements after
485 stroke induction. (c) Relative blood flow and pO_2 within the targeted regions dur-
486 ing and after photothrombosis. The green-shaded section indicates irradiation of
487 the targeted arteriole. The arrow indicates the propagation of an ischemia-induced
488 depolarization event.
489 6 Scale bars = 1 mm. Progression of the ischemic lesion over eight days as imaged
490 with (a) LSCI, (b) 445 nm tiled pO_2, and (c) 637 nm tiled pO_2 measurements. Day
491 -0 measurements were taken immediately prior to photothrombosis induction and
492 Day +0 measurements were taken immediately after. (d) Two arterioles (A1, A2),
493 one vein (V1), and two parenchyma regions (P1, P2) were targeted for chronic (e)
494 relative blood flow and (f) 445 nm pO_2 measurements (mean $\pm$ s.d.). The relative
495 blood flow was baselined against Day -0 measurements.